

ACTIVE EXTRAGALACTIC SOURCES: NEARLY SIMULTANEOUS OBSERVATIONS FROM 20 CENTIMETERS TO 1400 Å

ROBERT LANDAU, BILL GOLISCH, TERRY J. JONES, T. W. JONES, JEFFREY PEDELTY,
 LAWRENCE RUDNICK, AND MICHAEL L. SITKO
 University of Minnesota

JEFF KENNEY
 University of Massachusetts

TOM ROELLIG
 NASA Ames Research Center

ERKKI SALONEN AND SEppo URPO
 Helsinki University of Technology

GARY SCHMIDT
 University of Arizona

GERRY NEUGEBAUER, KEITH MATTHEWS, AND J. H. ELIAS
 Palomar Observatory, California Institute of Technology

C. IMPEY
 Division of Physics, Mathematics, and Astronomy, California Institute of Technology

AND

P. CLEGG AND S. HARRIS
 Queen Mary College, London

Received 1985 October 31; accepted 1986 February 14

ABSTRACT

Observations of 27 extragalactic sources have been made within a two-month period at wavelengths from 1400 Å to 20 cm. *IRAS* observations are given for 13 sources. Two groups of sources were observed: “active” sources, showing high variability, high polarization, or high 90-GHz fluxes, and a “control” group with low “activity” indicators. The spectra of the “active” sources are smooth with continuously changing slopes and no evidence for spectral “breaks” over more than six decades in frequency. In fact, simple parabolas in log flux density/log frequency space fit the data for the active (but not for the control) sources to ~10%–15%. Synchrotron models based on power law and Maxwellian particle energy distributions and the distribution derived from Fermi acceleration in shocks are compared to the observations of the “active” sources.

Subject headings: BL Lacertae objects — quasars — spectrophotometry

I. INTRODUCTION

The active extragalactic sources known as BL Lac objects, optically violent variables (OVVs), and the variable high polarization quasars (HPQs) are believed to offer the closest view of the central engine of quasar activity. These objects share the common properties of large amplitude and short time scale variability, high and variable polarization, and strong, variable radio emission. It is important to understand these common characteristics, to discover additional similarities, and to learn how these sources differ as a class from other objects such as the non-OVV flat spectrum radio sources and the radio quiet quasars.

Study of the spectral energy distributions across a wide frequency range can aid in this understanding by providing clues to the emission processes and energy production mechanisms at work. Of course, the large variability of the sources requires that the spectra be obtained nearly simultaneously. Indeed, outbursts which may occur are not only rapid but often confined to a specific frequency range (Robson *et al.* 1983; Balonek and Dent 1980), both of which can confuse the global spectral properties of a source unless thorough, nearly simultaneous observations are made.

Studies to date have provided valuable insights to a number of objects, but they have generally been limited either by small samples, by limited frequency coverage, or by the use of non-simultaneous measurements. Cruz-Gonzales and Huchra (1984) examined the nonsimultaneous radio to X-ray spectra of 25 BL Lac objects, finding complex but similar spectra. The QSO 1156+295 was observed extensively during an outburst (Glassgold *et al.* 1983; Wills *et al.* 1983). The resulting simultaneous spectra for this source are relatively smooth, although data are missing from the submillimeter through the infrared. Other individual objects, such as the N galaxy 3C 371 (Worrall *et al.* 1984a) and the BL Lac objects 0735+178, I Zw 187, OJ 287, 1418+546, ON 325, Mrk 501, and Mrk 180 (Bregman *et al.* 1984, 1982; Worrall *et al.* 1982, 1984b; Kondo *et al.* 1981; Mufson *et al.* 1984) have been the subject of focused simultaneous study from the radio through the ultraviolet and usually to the X-ray as well. Observations at 1 mm have been made, and the relationship between the millimeter and both the centimeter and the optical-infrared continua has been discussed by Jones *et al.* (1981) and by Ennis, Neugebauer, and Werner (1982). Landau *et al.* (1983) examined a sample of nine QSOs and BL Lac objects in the centimeter, millimeter, and optical

bands. In many of the studies above, the spectra obtained were discussed as combinations of power laws, but many times the data appear to be equally consistent with a smooth spectrum from the radio to the ultraviolet. Such a smooth spectrum was suggested by Harvey, Wilking, and Joy (1982) in the first submillimeter measurements of 3C 345.

To expand the number of objects studied nearly simultaneously at several frequencies, we have obtained measurements at up to 24 frequencies from the centimeter radio to the near UV on a sample of 19 objects which are strong millimeter-variable radio sources. In addition, a control sample of eight sources which differ in their centimeter radio properties was similarly studied. The combination of a relatively large number of sources, a control sample, and broad frequency coverage was designed to isolate and identify common properties.

II. OBSERVATIONS

The division of labor and dates of observation are given in Table 1. Most of the observations were made within the two-week period 1983 April 9–23, although the extreme range of the data presented here spans 11 weeks.

Our selection of objects was guided by the exploratory nature of these observations, since broad-band simultaneous measurements are so rare. We attempted to examine a variety of sources, instead of using a complete sample, at this stage. The bulk of our sources, which we call the “active” group, were selected for either strong emission from a compact component at 90 GHz ($\lambda = 3$ mm), or high optical polarization. These features often characterize active sources and distinguish them from other types of objects, such as radio-quiet or low-variability QSOs. Other studies of active sources have shown their overall spectral shapes to be quite uniform, with a “flat” radio spectrum and an effective power law slope around -0.7 from radio to optical frequencies. We therefore added eight sources to our observing list as a “control” group, using two different selection criteria. Four members of the control group were chosen because their radio spectra were not “flat,” but dominated by a single peak; these “peaked” sources have been

TABLE 1
JOURNAL OF OBSERVATIONS

Telescope	Wavelength(s)	Date (1983)
VLA	20, 6, 2, 1.3 cm	Apr 9–10
Metsähovi (13.7 m)	8 mm	Apr 12–29
FCRAO ^a (13.7 m)	3 mm	Mar 31–May 8
NRAO ^b (12 m)	3 mm	Apr 23–25, June 4–7
Hale (5 m)	1 mm	Mar 27, Apr 25–27
UKIRT (3.8 m)	350, 20, 10 μ m	Mar 29–Apr 4
IRAS	100, 60, 25, 12 μ m	Apr 15–May 24
Mount Jelma (2.3 m)	10 μ m	Apr 18
UKIRT (3.8 m)	1–3.5 μ m	Mar 29–Apr 14
Hale (5 m)	1–3.5 μ m	Apr 22–24
Mount Lemmon (1.5 m)	2.2 μ m	Apr 17–19
Mount Lemmon (1.5 m)	B, V, R	Apr 13–15
O'Brien (76 cm)	B, V, R	Apr 19
IUE ^d	2800–1400 Å	Apr 14–15

^a The Five College Radio Astronomy Observatory is operated with support from the NSF under grant AST-8026702 and with permission of the Metropolitan District Commission, Commonwealth of Massachusetts.

^b The NRAO and its VLA are operated by Associated Universities, Inc., under contract with the NSF.

^c Plus several upper limit observations in March and July.

^d The IUE satellite is sponsored and operated by NASA, by SERC, and by ESA.

identified by Rudnick and Jones (1982) as having less variability, and a similar group by Phillips and Mutel (1980) as having different VLBI structures than the active sources. The other four control group members were selected as having compact emission with much flatter radio-to-optical effective spectral indices than the active sources. This type source includes “radio-quiet” QSOs and the compact cores of extended radio sources. Finally, because of the uncertainty in the correction for galactic extinction in the optical, all sources were excluded if they were within 10° of the galactic plane. The entire source list is given in Table 2, along with references to earlier observations and designations for their respective selection criteria. (In what follows we define the spectral index, α by $S \propto \nu^{-\alpha}$).

Table 3 summarizes the observations of the 27 sources including the eight objects in the control group. Formal errors are shown, but a minimum error of 5% is used in the fitting (below). Upper limits (2σ) are indicated by “UL” in the error column. Not all sources were observed at all wavelengths; in particular, IUE observations were made for only five sources and IRAS measurements are given for only 13 sources. Two sources (0954+658 and 2021+614) lack optical and infrared measurements. (These sources were above the declination limit

TABLE 2
SOURCE LIST WITH CRITERIA FOR SELECTION AND REFERENCES TO PREVIOUS OBSERVATIONS

Source	Synonym	Selection Criteria	References
0735+178	...	mm ^a , pol ^b	1–5
0736+017	...	mm, pol	2–5
0829+046	OJ 049	pol	1, 2
0851+202	OJ 287	mm, pol	1–5
0906+430	3C 216	pol	2, 5, 6
0923+392	4C 39.25	C ^c :P ^d	3, 5, 6
0954+658	...	pol	5, 6
1156+295	4C 29.45	pol	6
1202+281	GQ Comae	C:L ^e	7
1219+285	W Comae	mm, pol	1–4
1226+023	3C 273	mm	1, 3, 4, 8
1253+055	3C 279	mm, pol	1–3, 8
1308+326	...	mm, pol	1–5
1351+640	...	C:L	3, 8
1418+546	OQ 530	mm, pol	1, 2, 4–6
1510–089	...	mm	1, 3, 5, 8
1514–241	AP Lib	mm, pol	1, 2
1538+149	4C 14.60	mm, pol	1, 2
1633+382	4C 38.41	mm	1, 4–6
1637+575	OS 562	C:P ^f	5, 6
1641+399	3C 345	mm, pol	1–6, 8
1704+608	3C 351	C:L	3, 8
1727+502	...	C:L	1, 2, 4
1749+096	...	mm, pol	1–5
1807+698	3C 371	pol	4–6
2021+614	OW 637	C:P	5, 6
2134+004	OX 057	C:P	5

^a Strong 90 GHz emission from a compact source.

^b Large or variable optical polarization (except 0954+658, selected for large polarization at 20 cm).

^c Control source.

^d Peaked radio spectrum.

^e Low ratio of radio to optical flux.

^f Although data from this paper show the radio spectrum unpeaked, this source appeared peaked from previous, less complete observations.

REFERENCES.—(1) Landau, Epstein, and Rather 1980; (2) Angel and Stockman 1980; (3) Ennis, Neugebauer, and Werner 1982; (4) Landau *et al.* 1983; (5) Rudnick and Jones 1983; (6) Rudnick and Jones 1982; (7) Sitko *et al.* 1982; (8) Neugebauer *et al.* 1979.

TABLE 3
MEASURED FLUX DENSITIES^a

Source	Log v: Synonym	9.176 20 cm	9.690 6 cm	10.176 2 cm	10.362 1.3 cm	10.568 8 mm	10.944 3 mm	11.477 1 mm	11.934 350 μ	12.477 100 μ	12.698 60 μ	13.079 25 μ	13.397 12 μ	Source
0735+178		1980 20	2200 5	2114 2	1941 10	2090 140	1730 250	2190 UL	1740 UL	333 UL	316 35	210 59	102 30	0735+178
0736+017		2160 10	2327 2	2668 6	2522 10	2140 240	1830 250	147 UL	158 20	147 UL	158 20	77 15	37 10	0736+017
0829+046	OJ 049	878 5	957 1	1235 3	1308 8	7370 160	6400 400	8090	4690 920	538 106	602 120	364 50	224 45	0829+046
0851+202	OJ 287	4600 20	4608 4	7243 12	7514 18	710 270	500 200			1276 85	824 90	458 15	190 23	0851+202
0906+430	3C 216	2923 200	1599 5	1062 4	918 7	710 270	500 200							0906+430
0923+392	4C 39.25	2601 100	5918 5	4051 8	3268 11	2250 100	1400 200			139 UL	45 UL	50 UL	30 UL	0923+392
0954+658		497 3	651 1	880 3	883 7	1120 230	600 200			175 UL	63 13	63 UL	39 UL	0954+658
1156+295	4C 29.45	1731 7	1729 2	1648 3	1634 8	1900 230	870 200							1156+295
1202+281	GQ Comae	7 UL	0.9 .3	2 UL		200 UL	90 UL							1202+281
1219+285	W Comae	1990 10	1870 1	1610 3	1510 10	1320 90	1630 150	4860 UL	2550 UL					1219+285
1226+023	3C 273	35340 530	29930 140	38920 80	34390 100	32590 430	41500 200	69900 10600	24370 2740					1226+023
1253-055	3C 279	9170 60	12080 10	10770 20	9830 40	9140 310	5400 500	3900 1000	1800 490	567 UL	235 UL	299 UL	209 UL	1253-055
1308+326		1440 30	1900 1	3015 4	3120 10	2950 140	2750 100	2800 1000	1380 540	529 UL	427 106	185 UL	190 UL	1308+326
1418+546		58 3	30 1	8.7 1.5	2.3 .3	400 UL	150 UL	5100 UL		1119 25	797 15	519 10	176 20	1418+546
1510-089	OQ 530	1407 14	1756 1	1735 5	1795 12	1480 90	1400 250							1510-089
1514-241	AP Lib	2400 200	2294 3	2343 6	2358 15	1870 160	1450 200							1514-241
1538+149	4C 14.60	1905 21	1837 2	1643 5	1564 11	1850 150	1360 130							1538+149
1633+382	4C 38.41	1571 13	1840 2	2199 5	3438 18	2560 110	2000 100							1633+382
1637+575	OS 562	2063 11	3310 3	3711 7	1441 9	1190 110	1000 110							1637+575
1641+399	3C 345	1170 20	1594 1	1416 3	15090 73	13420 300	10250 400	7400 1800	4270 790	1295 113	904 38	463 19	209 20	1641+399
1704+608	3C 351	7600 200	11260 12	15370 55	6.2 1.2	370 UL	100 30			337 UL	173 34	151 20	47 19	1704+608
1727+502		190 20	150 10	130 10	120 10	250 90	80 40			340 UL	119 UL	75 UL	70 UL	1727+502
1749+096		760 50	1086 1	2525 12	3119 24	3010 160	3050 200	2600 700	1500 UL	284 98	248 25	84 19	52 13	1749+096
1807+698	3C 371	1500 200	1626 4	1741 5	1793 10	1090 110	1250 150							1807+698
2021+614	OW 637	2270 30	2362 2	2224 6	1997 12	620 140	455 55							2021+614
2134+004	OX 057	4300 100	9700 8	6800 37	5400 37	2980 280	1510 160							2134+004

TABLE 3—continued

Source	Log ν : Synonym	13.176 20 μ	13.477 10 μ	13.903 3.75 μ	14.125 2.25 μ	14.230 1.65 μ	14.380 1.25 μ	14.633 7000Å	14.740 5500Å	14.845 4400Å	15.020 2860Å	15.230 1800Å	15.322 1440Å	17.683 2 KeV	Source	
0735+178														0.00023	0735+178	
0736+017															0736+017	
0829+046	OJ 049														0829+046	
0851+202	OJ 287														0851+202	
0906+430	3C 216	529 125	282 20	92.0 6.4	58.8 4.1	41.8 2.9	32.7 2.3	19.03 .25	14.25 .12	10.73 .11	5.2 .3	3.2 .2		0.0012	0906+430	
0923+392	4C 39.25														0.000115	0923+392
0954+658															0954+658	
1156+295	4C 29.45														1156+295	
1202+281	GQ Comae														1202+281	
1219+285	W Comae														1219+285	
1226+023	3C 273	1426 99	447 28	179 12	91.4 6.4	50.2 3.5	38.0 2.6	33.7 .5	31.8 .3	28.9 .3	24.4 1.2	15.3 0.7	12.4 0.6	0.00832	1226+023	
1253-055	3C 279	205 UL	42 8	9.7 2.0	5.3 1.1	3.3 .7	2.3 .5	1.97 .10	1.2 ^a .02	0.90 .03				0.00027	1253-055	
1308+326		241 53	78 10	28.8 2.0	16.4 1.1	11.5 .8	9.5 .7	3.62 .30	2.58 .10	1.72 .10				0.00020	1308+326	
1351+640															0.000030	1351+640
1418+546	OQ 530														1418+546	
1510-089															1510-089	
1514-241	AP Lib														1514-241	
1538+149	4C 14.60														1538+149	
1633+382	4C 38.41														1633+382	
1637+575	OS 562														1637+575	
1641+399	3C 345	353 76	111 13	36.6 2.5	18.4 1.6	11.8 .8	7.7 .5	3.21 .07	2.50 .03	1.87 .03				0.00025	1641+399	
1704+608	3C 351														0.000035	1704+608
1727+502															0.00148	1727+502
1749+096															0.00025	1749+096
1807+698	3C 371														0.00042	1807+698
2021+614	OW 637														2021+614	
2134+004	OX 057														2134+004	

NOTES.—The X-ray data for the sources 0923+392, 1202+281, 1226+023, 1253-055, 1351+640, 1641+399, and 1704+608 were taken from Tannanbaum *et al.* 1983. The equivalent 2 keV for all other sources were taken from Ledden and O'Dell 1985 reporting on original references as follows: 0735+178, Bregman *et al.* 1984; 0851+202, 1219+285, and 1308+326, Madjeski and Schwartz, 1983; 1727+502, Bregman *et al.* 1982; 1749+096, Ledden and O'Dell's own work; and 1807+698, Worrall *et al.* 1984.

^a In millijanskys.

of the Mount Lemmon telescope, and the other telescope that was to have observed them was clouded out.) They will not be discussed further.

Individual observations, including centimeter polarization data, are available from the authors. Details of the observing procedures, calibration and data reduction at the different wavelengths are given below.

a) Centimeter Observations

Observations at $\lambda = 20, 6, 2,$ and 1.3 cm were made at the Very Large Array (VLA) on 1983 April 9–10. The array was in its C-configuration, with maximum baselines of ~ 4 km. The data were calibrated on the scale of Baars *et al.* (1977), using 3C 286. Integration times were typically 2, 2, 6, and 10 minutes at $\lambda = 20, 6, 2,$ and 1.3 cm. The quoted flux values were derived from simple averages of all visibility points (but see below), along with formal rms errors. Additional uncertainties of approximately 1.5%, 0.7%, 3%, and 3%, respectively, result from the calibrations.

Plots of visibility amplitude versus baseline length were examined for all sources at $\lambda = 20$ and 6 cm, to look for possible contamination by extended features. In cases where the shortest baseline visibilities exceeded the longest by $\sim 5\%$ or more, maps were made, and the flux values quoted refer to the peaks on the maps. Typical beam sizes were $\sim 13''$, ($4''$) for $\lambda 20$ (6 cm). In the case of 1704+608 (3C 351), the core could not be well separated from the strong extended emission at $\lambda 20$ cm. We also made maps of the weak sources 1202+281 and 1351+640 to verify that our visibility average represented flux from unresolved features.

b) 8 Millimeter Observations

Observations at 36.8 GHz were made with the Metsähovi 13.7 m telescope of the Helsinki University of Technology's Radio Laboratory. Sources were observed 1–8 times (almost all were observed at least twice) with an on-on method using typically an on-cycle time of 20–30 s and a total integration time of 800–2000 s. A heterodyne two-beam receiver with a 1 GHz bandwidth and a system noise temperature of 1200 K was used. The beam separation was $6'$ (2.5 times the HPBW), and the chopping rate was 25 Hz.

DR 21 was the primary calibrator with an assumed flux density of 18.0 Jy at 36.8 GHz. A noise diode calibrator was used for the secondary calibration. The optical depth of the atmosphere was measured using the "tipping" method of Fogarty (1975) every 4–6 hours. Atmospheric changes in the direction of the source were monitored by a sky radiometer operating at 22 GHz. Observations during unstable weather conditions were cancelled. The fluxes in Table 3 are the weighted mean of the individual observations, and the errors (where shown) include the statistical errors of the observations and calibrations and the errors of the values of the optical depth. Further details of the observing and reduction techniques are presented in Salonen *et al.* (1983).

c) 3 Millimeter Observations

Fourteen of the sources were observed in April with the Five College Radio Astronomy Observatory 13.7 m telescope. A few observations were made in April by Bill Cotton and some by Paul Rhodes at the resurfaced NRAO 12 m and all but three sources were also observed in early June at the 12 m by Rick Howard. Observations of almost all sources measured more than once agreed to within 10%. The fluxes in Table 3 are

weighted means, and the errors are the larger of the discordance of separate measurements or the statistical errors of the measurement plus calibration.

Observations at the Five College Radio Astronomy Observatory were made with a cooled heterodyne receiver operating between 84.8 and 91.3 GHz. The receiver was a cooled Schottky diode mixer with 1.4 GHz intermediate frequency GaAs field effect transistor (FET) amplifiers of 400 MHz bandwidth. Double sideband system temperatures ranged from 200 to 300 K; the aperture efficiency had an average value of 0.38. On-on switching was employed with a 15 Hz chopping rate and a $7'$ throw-in azimuth.

Five calibrators were used, at least two each night: Venus, Jupiter, Saturn ($T_b = 367$ K, 179 K, and 149 K, respectively, at 90 GHz; Ulich 1981) and DR 21 and 3C 274 ($F_v = 16.9$ Jy and 8.3 Jy, respectively, at 90 GHz; Balonek 1982). Both the pointing and the calibration were checked at least hourly.

Measurements made at NRAO used Venus as the calibrator in April and Saturn in June; brightness temperatures are as above.

d) 1 Millimeter and Submillimeter Observations

The 1 mm continuum observations were made at the 5 m Hale telescope on 1983 March 27 using the He³ bolometer system described in Roellig and Houck (1983). Upper limits for 0735+178, 0851+202, and 1219+285 were obtained on 1983 April 25–27. All of the observations were made with a measured beam diameter of $55''$ and through airmasses less than 2. The 350 μ m observations were made at the UKIRT 3.8 m telescope during 1983 March 29–April 4 using a recently developed He³ bolometer system similar to that described above. The observations were made through bandpass filters (295–385 μ m) isolating the 350 μ m atmospheric window and used a focal plane aperture that gave a measured beam diameter of $39''$ on the sky. The objects were observed through airmasses of less than 1.6 and on more than one night in order to reduce possible systematic errors. Standard infrared chopping techniques with chopper throws of at least one beam diameter were used for background subtraction. For both the one millimeter and submillimeter observations the data were reduced using the techniques outlined in Elias *et al.* (1978), including bandpass and beam-size corrections, with Jupiter taken as the primary standard. The Jovian brightness temperature was taken from Werner *et al.* (1978) and Cunningham *et al.* (1981) as 168 K and 147 K for the 1 mm and 350 μ m observations, respectively. Water vapor along the line of sight was estimated from the signal strengths of standards and extinction curves on the more stable nights.

e) IRAS Observations

Ten of our sources were observed by the IRAS satellite in "pointed" mode (Neugebauer *et al.* 1984) during late March, April, and May. In five cases no individual observation produced a detection, so the pointed observations were co-added to increase the sensitivity. These cases are 0735+178 (four observations), 0736+017 (10), 0923+392 (11), 1156+295 (10), and 1749+096 (four). Upper limits on two additional sources (1253–056 and 1308+326) were obtained by co-adding the IRAS survey data at the positions of these sources. All IRAS upper limits are 3 times the mean noise level as determined in the 1.5×0.5 field of the pointed observations.

For 0851+202 and 1351+640 enough individual observations were available (five and 11, respectively) to calculate

uncertainties from the observations. In the other cases, the uncertainties were based on the fluctuations in the background levels of the pointed observations; these typically ranged from 10% to 25%.

Extensive observations of 1641+399 (3C 345) were made with *IRAS* both in 1983 February–March and in 1983 July–September (Bregman *et al.* 1985). The observations showed a smooth decline by factors of 1.7 ± 0.3 , 1.6 ± 0.2 , 1.3 ± 0.1 , and 1.1 ± 0.1 at 12, 25, 60, and 100 μm , respectively, between the two periods. For the present study, flux densities obtained by an appropriate interpolation between the early and late values were assumed.

Flux densities have not been color corrected because the corrections are less than 1%. Further details of the data reduction and calibration can be found in the Supplement to the *IRAS* Catalog (Beichman *et al.* 1984).

f) 10 Micron and 20 Micron Observations

Observations at UKIRT were made during the same time period as the submillimeter observations. The focal plane aperture was 10" in diameter and the chopper throw was 1'. Bright stars from the list of Tokunaga (1984) were used for calibration with adopted zero-magnitude fluxes of 37 Jy at 10 μm and 10 Jy at 20 μm .

The 10 μm point for 1202+281 was obtained by Gary Grasdalen using a Ge bolometer on the Mount Jelma 2.3 m telescope.

g) Near-IR Observations

The near infrared (1–4 μm) photometry was done on three different telescopes with slightly different photometric systems on each. The UKIRT observations were made during the same run as the millimeter observations with facility equipment. An 8" aperture with a 1' chop was used. The Hale 5 m observations were made on April 22–24 with 5" aperture and a 15" chop. Twenty sources were measured at K on the University of Minnesota–University of California, San Diego 1.5 m telescope on Mount Lemmon using an 18" aperture and a 30" chop during April 17–19. The photometric standards given in Elias *et al.* (1982) were used by all three observing teams.

The photometric magnitudes were first converted to millijanskys at the effective wavelengths of the filters for each photometer. For example, the effective wavelength of the Caltech *J* filter is 1.27 μm but the effective wavelength of the UKIRT *J* filter is closer to 1.20 μm . The absolute calibration given by Hayes (1979) was used to compute fluxes. The fluxes for α Lyr tabulated in Kurucz (1979) were used to interpolate between the wavelengths given in Hayes. These fluxes were then adjusted to a common set of wavelengths using the average spectral slope between 1.2 and 3.8 μm for the sources. These wavelengths are 1.25, 1.65, 2.25, and 3.75 μm and were chosen to lie between the effective wavelengths of the various photometric systems.

A comparison of the fluxes from six sources observed at K at both Mount Lemmon and at UKIRT and of four sources observed at Hale and at UKIRT indicate that even for bright sources measured with a few percent internal accuracy the discrepancy is 5%–10%. We think this is largely due to intrinsic source variability, although systematic differences between observatories may contribute. Consequently, we have assigned 7% errors to all sources at 1.25, 1.65, 2.25, and 3.75 μm . Where a source was observed at both Hale and UKIRT the Hale

fluxes were used because they were made closer to the date of most other observations.

In the case of 1253–055 (3C 279) the 1–4 μm fluxes measured at Hale changed by ~ 0.25 mag between April 22 and 23. Neither 3C 273 nor 3C 345 varied during this time. We therefore have no accurate idea of the flux one week earlier when the optical observations were made. Consequently we have given 20% errors to these points. (They could have been assigned to the optical data with equal justification.)

A discrepancy of 30% exists in the case of 1749+096 between observations made two weeks apart. Again, these data are given errors of 20%.

h) Optical Observations

Observations at 4400 Å (*B*), 5500 Å (*V*), and 7000 Å (*R*) were carried out on the Mount Lemmon 1.5 m telescope using the dual-channel Two-Holer GaAs polarimeter/photometer operating in its two-aperture photometric mode (see the brief description in Sitko, Schmidt, and Stein 1985). Twin 16" circular entrance apertures separated by 88" were used except where contamination required the use of 8" holes. Beam switching between the apertures was done every 30 s. Landolt (1973) standard stars with *R* photometry by Kunkel and Rydgren (1979) were used to transform to the Johnson standard system. Extinction coefficients were calculated each night, and the residuals of the transformation were 0.025 mag or smaller. Each source was measured several times through each channel, and most sources were measured on more than one night. Corrections for galactic absorption were calculated based on the data of Burstein and Heiles (1982). The errors in Table 3 are the combined errors in the photometry, in the transformation, in the correction for galactic absorption, and where the smaller aperture was used for the aperture correction. The conversion from magnitude to absolute flux density is based on Tüg, White, and Lockwood (1977).

Additional observations of 1807+698 (3C 371) as well as 3C 273 were made at the University of Minnesota's O'Brien Observatory 76 cm telescope. Extinction values were chosen to minimize residuals of the transformation (at 0^m04), and the conversion to absolute fluxes used the values from Puschell (1978). After reduction the fluxes for 3C 273 agreed with those measured at Mount Lemmon. Subtraction of the galaxy component of 1807+698 was made using the data of Sandage (1973). Errors of 20% were assigned to the fluxes to reflect the uncertainty of this subtraction.

Observations of 1351+640 at *B* and *V* were made on April 18 by W. Z. Wisniewski using 1P21 photomultiplier at the Lunar and Planetary Laboratory's 1 m telescope on Mount Lemmon.

i) Ultraviolet Observations

All of the ultraviolet data were obtained by one of us (M. L. S.) using the *International Ultraviolet Explorer* (*IUE*) satellite using both the shorter wavelength SWP and longer wavelength LWR cameras. All of these observations were made in the low resolution mode using the large entrance aperture. Absolute fluxes were estimated from the Calcomp plots provided by the standard Goddard reduction package. The fluxes were measured at three frequencies: $\log \nu_{\text{HZ}} = 15.02$ (2865 Å), 15.22 (1808 Å), and 15.32 (1436 Å) and corrected for extinction. The absolute flux calibration used is that of Holm and Rice (1981).

j) X-Ray Observations

Although we did not obtain X-ray data as part of this program, we have added measurements from the literature to Table 3 and to the plots in Figure 4. References for these data are included in the notes to Table 3. In all cases, we have preserved the corrections made by the original authors for hydrogen absorption in our galaxy and their normalization assuming a power-law (slope = -0.5) X-ray spectrum. We have converted all measurements to a monochromatic flux at a common observed energy of 2 keV, before plotting them in the rest-frame coordinates of Figure 4. No errors have been assigned to these X-ray data because of the unknown effects of variability. The calibration errors are dominant and can lead to uncertainties of up to 25% (Tannanbaum *et al.* 1983).

III. RESULTS

The spectra were transformed to the rest frame of the source by multiplying the flux densities of Table 3 by $(1+z)^2$ and multiplying all frequencies by $(1+z)$. For this purpose the

five BL Lac objects for which no redshifts were available were assigned the redshift 0.50, similar to that of several other BL Lac objects with measured redshifts. The resulting spectra are displayed in Figure 1, where the log of the rest frame flux density, S_ν , is plotted against the log of the rest frequency, ν . The spectra of most sources are smooth, with no spectral "breaks" over six decades in frequency. The sources with the best wavelength coverage are the best examples; sources with poorer coverage are consistent with this interpretation of smoothness, but do not require it. The local slopes of these smooth spectra vary continuously from 0 (or slightly positive) in the radio to between -1 and -1.5 in the optical. In most cases even the "flat" radio portions of the spectra show the convex curvature.

The simplest smoothly curving function is a parabola; we therefore fit all spectra by weighted least squares to a quadratic function of the form

$$\log S_\nu = C + (\log \nu - B)^2/2A. \quad (1)$$

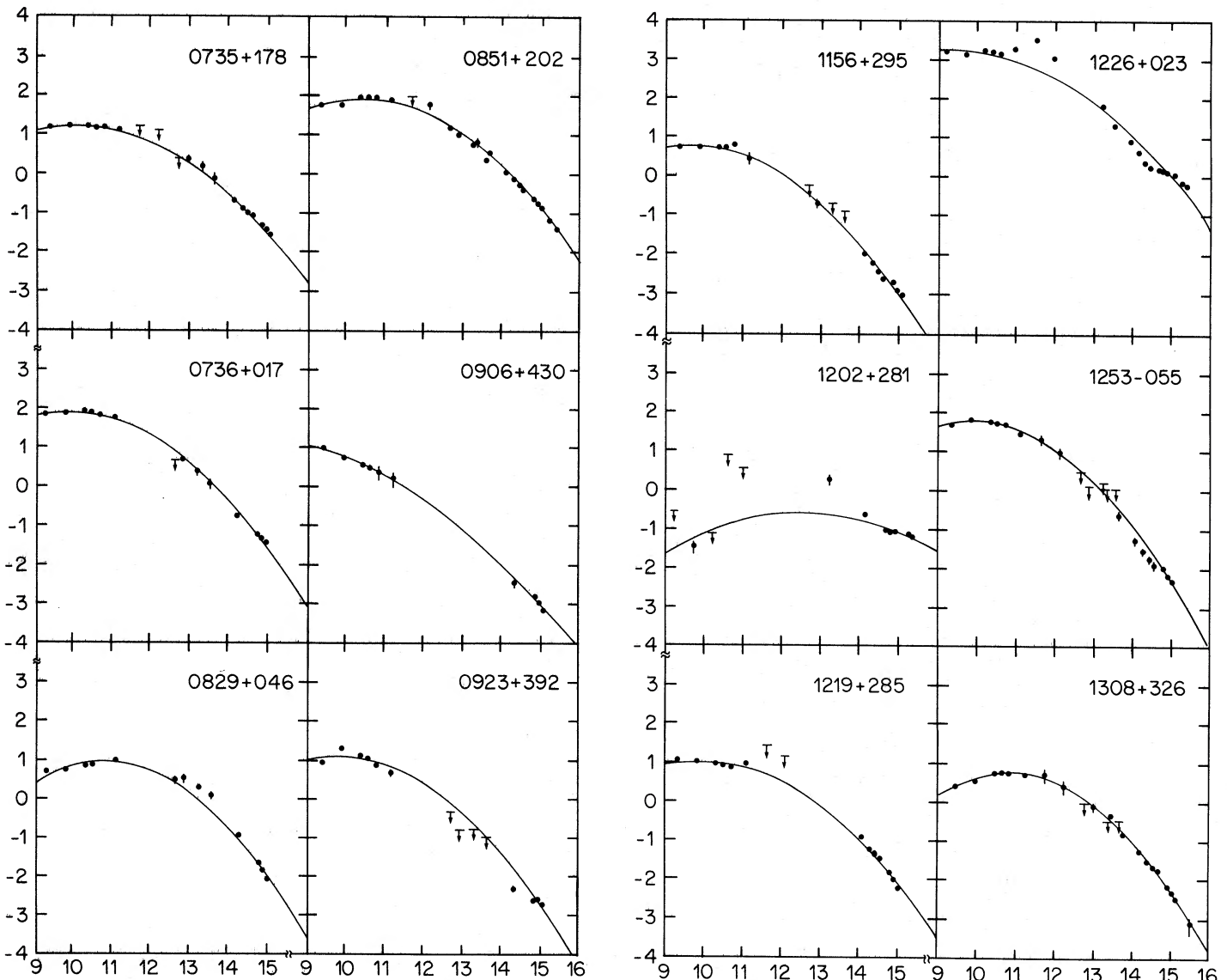


FIG. 1.—Broad-band spectra of 25 extragalactic sources, redshifted to the rest frame of the source. The log of emitted flux density in arbitrary units is plotted as filled dots against the log of frequency in Hz. The solid curves are the best fit to a logarithmic parabola.

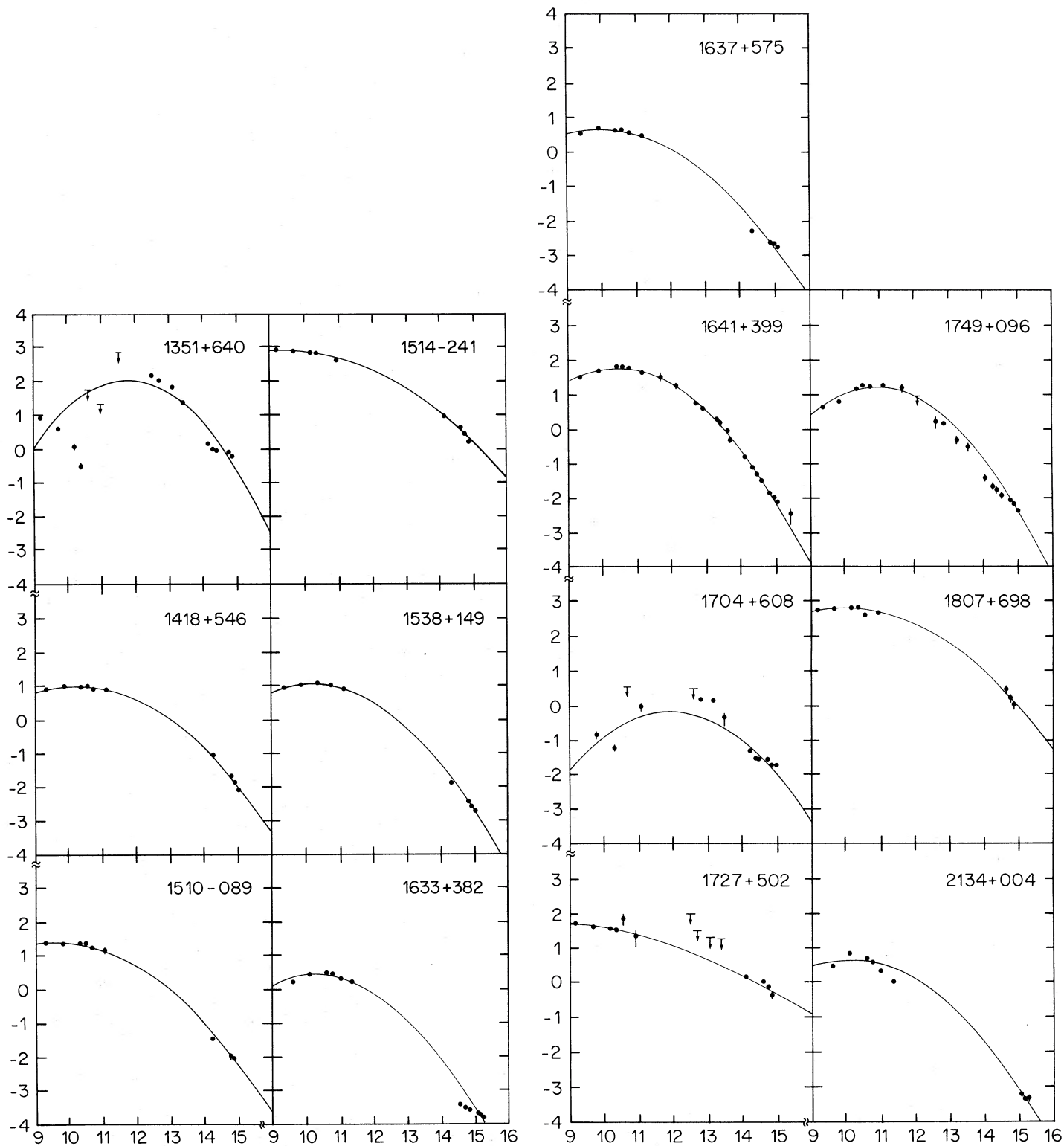


FIG. 1—Continued

TABLE 4
PARAMETERS OF THE PARABOLIC FITS

Name	Synonym	z	A	B	C	$\chi^2/\text{Degrees of Freedom}$
0735+178.....	...	0.42	-4.50	9.96	-0.11	1.42
0736+017.....	...	0.19	-3.81	9.82	-0.89	5.24
0829+046.....	OJ 049	0.50	-2.96	10.85	-0.06	14.45
0851+202.....	OJ 287	0.31	-3.80	10.32	0.03	6.09
0906+430.....	3C 216	0.67	-7.38	6.94	0.93	1.76 ^a
0923+392.....	4C 39.25	0.70	-3.56	9.78	0.73	36.12 ^b
1156+295.....	4C 29.45	0.73	-3.76	9.65	0.47	7.92
1202+281.....	GQ Comae	0.17	-5.88	12.56	-3.57	22.14 ^b
1219+285.....	W Comae	0.50	-4.03	9.99	0.02	10.88
1226+023.....	3C 273	0.16	-5.04	9.21	0.19	70.29 ^a
1253-055.....	3C 279	0.54	-3.22	9.87	0.89	4.85
1308+326.....	...	1.00	-2.86	10.84	1.07	1.66
1351+640.....	...	0.09	-1.92	11.79	-2.08	320.00 ^b
1418+546.....	OQ 530	0.50	-3.71	10.29	0.0	5.24
1510-089.....	...	0.36	-4.05	9.59	-0.21	10.22
1514-241.....	AP Lib	0.05	-5.64	9.45	-2.29	9.91
1538+149.....	4C 14.60	0.50	-3.09	10.12	0.05	5.04
1633+382.....	4C 38.41	1.81	-2.79	10.29	1.92	50.23 ^a
1637+575.....	OS 562	0.75	-3.76	9.95	0.40	19.56 ^b
1641+399.....	3C 345	0.60	-2.72	10.41	1.09	4.17
1704+608.....	3C 351	0.37	-2.50	11.98	-1.69	39.45 ^b
1727+502.....	...	0.06	-12.65	7.81	-3.06	2.00 ^b
1749+096.....	...	0.50	-2.29	10.94	0.18	14.02
1807+698.....	3C 371	0.05	-4.48	9.95	-2.33	3.30
2134+004.....	OX 057	1.94	-3.28	10.10	2.31	36.39 ^b

NOTES.— $z = 0.50$ assumed for 0829+046, 1219+285, 1418+546, 1538+149, and 1749+096.

^a Anomalies (see text).

^b Control group.

The meaning of the parameters is: C is the log of the peak emitted flux density, B is the log of the frequency at which this maximum occurs, and A , the “curvature” parameter, is the interval in $\log \nu$ from the peak, B , to the place where the spectrum has a slope of unity. The X-ray data have *not* been included in the fit because they were not simultaneous with the rest of the data. These best-fit parabolas are plotted as solid lines in Figure 1. The parameters A , B , and C are listed in Table 4 along with the reduced χ^2 of the fit; that is, $\chi^2/(n-3)$, where n is the number of data points.

There are several ways to characterize the fit of the curves to the data; we chose two: visual inspection and the reduced χ^2 . Moreover, we ask whether a homogeneous group of sources stands out characterized by some property of the fits and, if so, how is this group related to our active and control groups?

Visual inspection, although somewhat subjective, has the advantage of generality: peculiarities of individual fits and relationships among fits can be discerned without specifically programming the inspector. The χ^2 method is objective but has several disadvantages as used here. The most important of these follows from the fact that we are not proposing the parabola of equation (1) as an exact mathematical model of the sources' behavior. (For example, there is no reason to expect that departures of the data from the parabola will be normally distributed.) We ask whether equation (1) describes the *global* properties of the spectra, notwithstanding departures from the parabola at localized frequencies. An investigation of these departures is a second-order (and perhaps a profitable) study. One or two “bad” points in a spectrum can provide most of the contribution to a large reduced χ^2 even though the fit is globally “good.” Incompletely known systemic errors at some wavelengths and the difficulty in maintaining an absolute flux calibration across technologies (across frequencies) are a few of the expected problems.

Visual inspection of Figure 1 results in the following classification into good and bad fits: all of the active group are well fitted except 1226+023 and 1633+382 and perhaps 1253+055 and 1749+096. None of the control group is well fitted except perhaps 1637+575. All the authors made the same evaluation except at most for the few borderline cases. More importantly, a homogeneous group stands out comprising all of the active group except for 0906+430, 1226+023, and 1633+382 and characterized by well fitted parabolas of approximately the same curvatures and peak frequencies.

The reduced χ^2 values from Table 4 divide the sources as follows: all the active group have small χ^2 except 1226+023 and 1633+382 and perhaps 0829+046 and 1749+096. All of the control group have large χ^2 , except 1727+502. This is substantially the same division that visual inspection provided.

There are perhaps reasons (admittedly after the fact) why the two worst-fit sources in the active group, 1226+023 and 1633+382, ought not to have been included in the “active” sample. The source 1226+023 (3C 273) is only 0.3% polarized in the optical. All the other sources in our “active” group for which we have such data are polarized between 2% and 16%. Furthermore, 3C 273 experienced a submillimeter/millimeter radio outburst which began in 1983 (Robson *et al.* 1983). This appears to have been localized in frequency, which therefore temporarily distorts the broad-band spectrum. The other poorly fitting active source, 1633+382, has an unusually low polarization at 20 cm. Only one other source, 0906+430, has such a low polarization; all the other active sources are polarized between 1.2% and 7% at 20 cm. Although 0906+430 is well fitted by equation (1), we see from Table 4 that its values of A and B are well outside the range for the other sources, and Figure 1 shows a steep radio spectrum, uncharacteristic of the other “active” sources. In order to *define* a homogeneous set of sources for further discussion we will classify 0906+430,

1226+023, and 1633+382 as “anomalies” and use the word active to refer to the other 15 active sources, all of which are fitted by a smooth parabola. The two worst-fit sources in this homogeneous group are 0829+046 and 1749+096 because of the departure of the curves from the *IRAS* data. For the former source, *IRAS* measurements in October are significantly lower than those of May. No later observations of 1749+096 are available.

The difference in results between the active and control groups is not surprising because these two groups were chosen to be different. What is (perhaps) surprising is how well all but three of the 18 chosen active sources were fitted by equation (1).

a) Significance and Selection Effects

In Figure 2 we present histograms of the parameters *A*, *B*, and *C*. We have made several tests of the significance of the

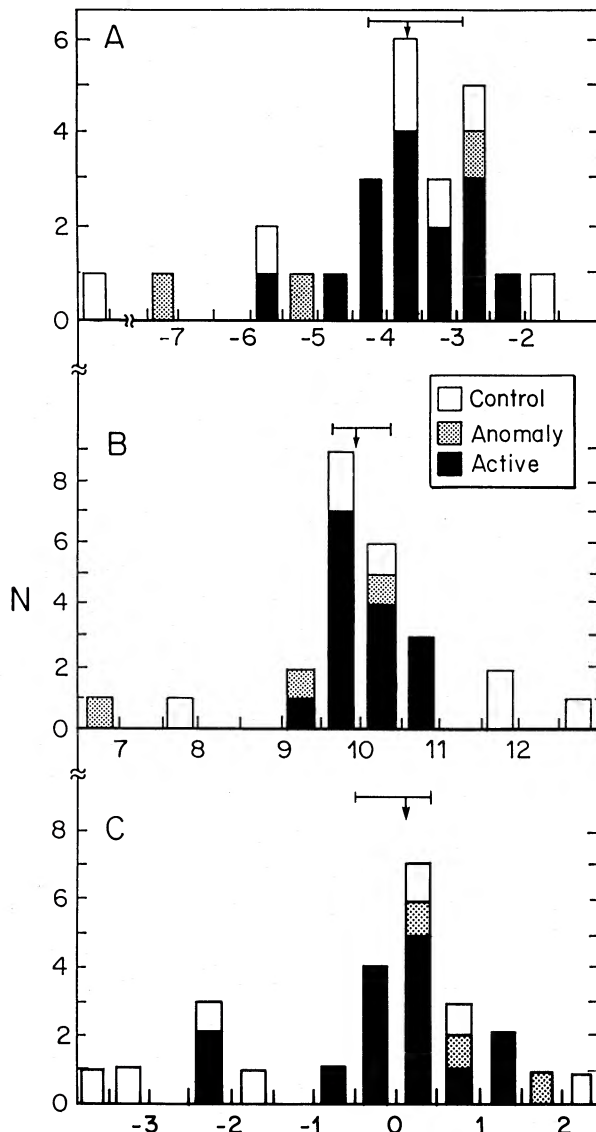


FIG. 2.—Histograms of the parameters of the parabolic fits of eq. (1). The arrows and the horizontal lines indicate the median and interquartile range of the active sample (not including “anomalies”).

parabolic fits and of the extent to which they may result from selection. Many of the sources’ spectra were fit to least-squares cubics. The best-fit cubics were in almost all cases the same as the best-fit parabolas; that is, there were no other global features of the spectra to be fitted by making use of the extra degree of freedom.

We also divided each spectrum into halves at the gap between 20 μm and 350 μm , omitted the *IRAS* data, and produced a set of 120 “scrambled sources” by combining each radio half of a spectrum, in turn, with all other optical half-spectra. The two halves were not corrected or normalized in any way. We then compared the values of χ^2 from fits for the “scrambled sources,” to the values for the true sources. For those sources (such as 1308+326) with fairly complete wavelength coverage, the reduced χ^2 of the fits of the scrambled “sources” increased by typically an order of magnitude. Thus we have evidence that for these sources the optical and radio fluxes are closely related. For sources (such as 1418+546) with a large gap in coverage in the IR/submillimeter region, the reduced χ^2 increased by only a factor of 2 (typically) when their “scrambled” versions were examined. For these latter sources, selection from a radio-loud sample with measurable optical flux is sufficient to produce some acceptably parabolic fit to the spectrum.

Finally, we increased the errors of each data point until the reduced χ^2 (for actual source fits) was lowered to a value of 2. We found this typically occurred when the errors were made 10%–15%. Thus the parabolas are a good fit to the *global* properties of the sources at a level of 10%–15%. The parabolas are not good fits to any structures in the spectra that are confined to less than a decade in frequency. Furthermore, we are not suggesting that a quadratic function in $\log \nu$ is a unique mathematical representation of the spectra; merely that whatever function is predicted by a physical model of the source should have a polynomial approximation that is good to $\sim 10\%$ –15% in second order.

b) Properties of the Parabolas

Correlations.—Figure 3 shows scatter diagrams of the parameters *A*, *B*, and *C* for the 15 active sources. It is seen that *A* (the “width” of the parabola) is correlated with the peak frequency, *B*, and flux *C* (respective Spearman rank correlation coefficients $r_s = 0.77$, 0.78 , confidence levels $>99\%$). The parameter *C* is slightly correlated with *B*, ($r_s = +0.49$, confidence level $\geq 90\%$, respectively). Implications of these correlations are deferred to § IV. The active sources also seem to be a more homogeneous group than the controls, since their distributions of *A*, *B*, and *C* appear narrower (Fig. 2). To test this quantitatively, we generated the lists of $|X - \text{median } X|$, where $X = A, B$, or C , for both active and control groups. We then performed a rank sum test on these lists and found that the active distributions of *B* and *C* are narrower than the controls (at 95% confidence) but the actives are only marginally narrower (83% confidence) for *A*.

Emitted energy.—Integrating equation (1) over frequency gives the emitted energy. (No additional flux contribution for X-rays is being made.) Because of the correlation between *B* and *A*, the peak energy always is emitted near 10^{14} Hz. Most of the parabolas have *A* between -3 and -4 . For $A = -3$ and $B = 10.7$ (the value implied by the correlation of Fig. 4a) we find half the energy is emitted between $1 \mu\text{m}$ and $40 \mu\text{m}$ with the peak at $7 \mu\text{m}$. For $A = -4$ (and $B = 10.2$) we find half the energy between $0.3 \mu\text{m}$ and $16 \mu\text{m}$ with the peak at $2 \mu\text{m}$.

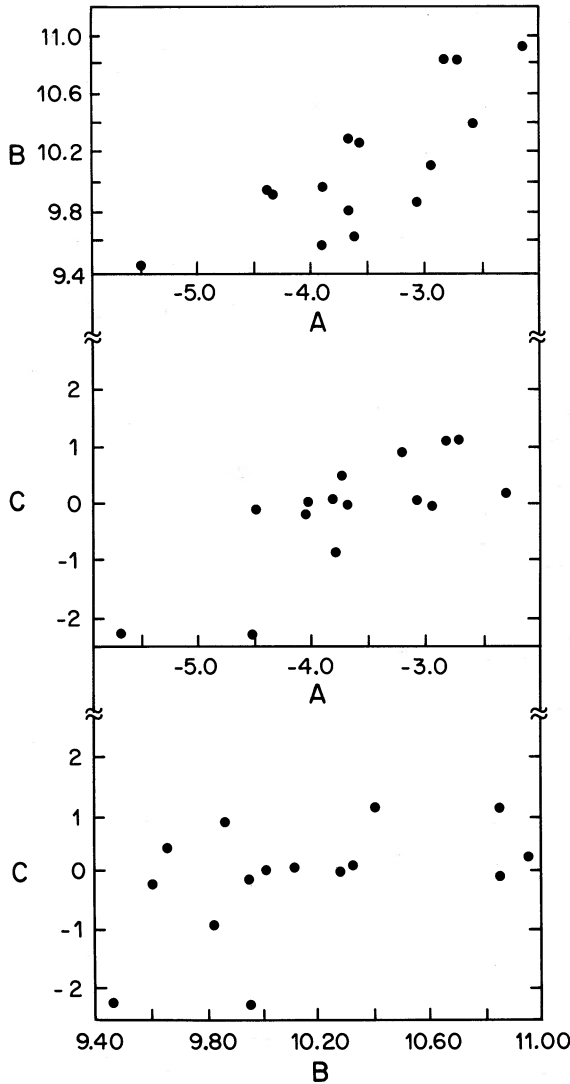


FIG. 3.—Correlations among the parameters A , B , and C for the 15 active sources (indicated by filled dots). Correlation coefficients are given in the text [§ III(b)].

Although much of the energy is emitted in the infrared, a large fraction also comes out in the optical.

Extrapolations.—Figure 4 shows the parabolic fits extrapolated to the X-ray region for the eight active sources for which X-ray data are available (see also Table 3). For several of the sources, e.g., 0735 + 178, 0851 + 202, 1807 + 698, the extrapolated parabolas that were fitted from lower frequency data, provide quite good matches with the observed X-ray values. In other cases, a power-law extrapolation from the optical or near-IR would produce a closer match. At this point, we do not suggest that a parabolic extrapolation to the X-ray data is either demanded by the data or justified on theoretical grounds; a similar degree of skepticism should be applied to any power-law extrapolations found in the literature.

IV. DISCUSSION

a) The “Active” Sample

It is remarkable that so many source spectra are well fitted by a single three-parameter curve. This fact undoubtedly is

telling us something about the similarity in the structures of the sources, or about the relativistic particle energy distributions, or about both of these. However, only for the sources with good wavelength coverage are we justified in examining detailed models for the spectra. For the other sources, we can only say that our selection procedure has isolated spectra of a common type; the parameters of any fit (parabolic or otherwise) can only be considered as characteristic of the type, and we are not justified in comparing parameters between sources or between temporally separated observations of the same source. This same caveat applies to all analyses of spectra where there are large gaps in the wavelength coverage. We suggest that the test described above, involving simulated “scrambled” spectra, be performed whenever detailed models are under investigation.

The discussion below is therefore restricted to the sources with good wavelength coverage, for which we are confident that the derived parabolic curves are a good and significant representation of the data.

The simplest approach to analyzing this result would be to suppose that the parabolic fitting curve directly reflects the relativistic electron energy distributions. Of course, that is strictly meaningful only in a homogeneous, transparent source. These constraints are almost certainly not met at radio frequencies but become increasingly likely at wavelengths shorter than the millimeter. We begin there. A simple relationship can be derived between the shape of an emitted synchrotron spectrum and the electron energy distribution responsible for it. If $\alpha(\nu) = -d \log S/d \log \nu$ is the *frequency-dependent* spectral index of the emissivity S , a straightforward generalization of standard formulae gives at any frequency ($\nu = \text{const}$):

$$\int_0^{\infty} \left[2\alpha(\nu) + 1 + \frac{d \log n(\gamma)}{d \log \gamma} \right] n(\gamma) F(x) dx = 0, \quad (2)$$

where $n(\gamma)$ is the electron energy distribution and $F(x = \nu/\gamma^2 \nu_{B,L})$ is the monoenergetic emissivity. For power-law spectra ($\alpha = \text{const}$), this is satisfied by the usual $s \equiv d \log n/d \log \gamma = -(2\alpha + 1)$. For our logarithmic parabola (eq. [1]), $\alpha = -\log(\nu/\nu_{\max})/A$, where $\log \nu_{\max} = B$ and equation (2) is satisfied by the distribution

$$\log \left(\frac{n}{n_0} \right) = \frac{2}{A} \left[\log \left(\frac{\gamma}{\gamma_0} \right) - \frac{A}{4} \right]^2 - \frac{A}{8} \quad (3)$$

(with $\gamma_0^2 = \nu_{\max}/\nu_{B,L}$), which is also a logarithmic parabola. Formally, therefore, equation (3) is a suitable underlying energy distribution. This distribution is plotted in Figure 5 along with several other curves (described below) that may be useful to compare to it. We looked for physically reasonable electron energy distributions which would produce the synchrotron emissivity of equation (1). (Currently there is no theory which predicts a logarithmic parabola particle distribution.) Figure 6 illustrates the synchrotron emission spectra produced by each electron energy distribution of Figure 5, plotted so as to be the best-fit (as measured by eye) to the logarithmic parabola.

The simplest description of the observed spectra is one of continuously increasing (negative) slope to high frequencies. A simple and physically plausible energy distribution which produces an emissivity with this characteristic is the relativistic Maxwellian (Jones and Hardee 1978). Some success has previously been achieved in fitting the centimeter and millimeter spectra of sources similar to those in our sample (Spangler 1980; Barvainis 1984). However, as Figures 5 and 6 illustrate, a

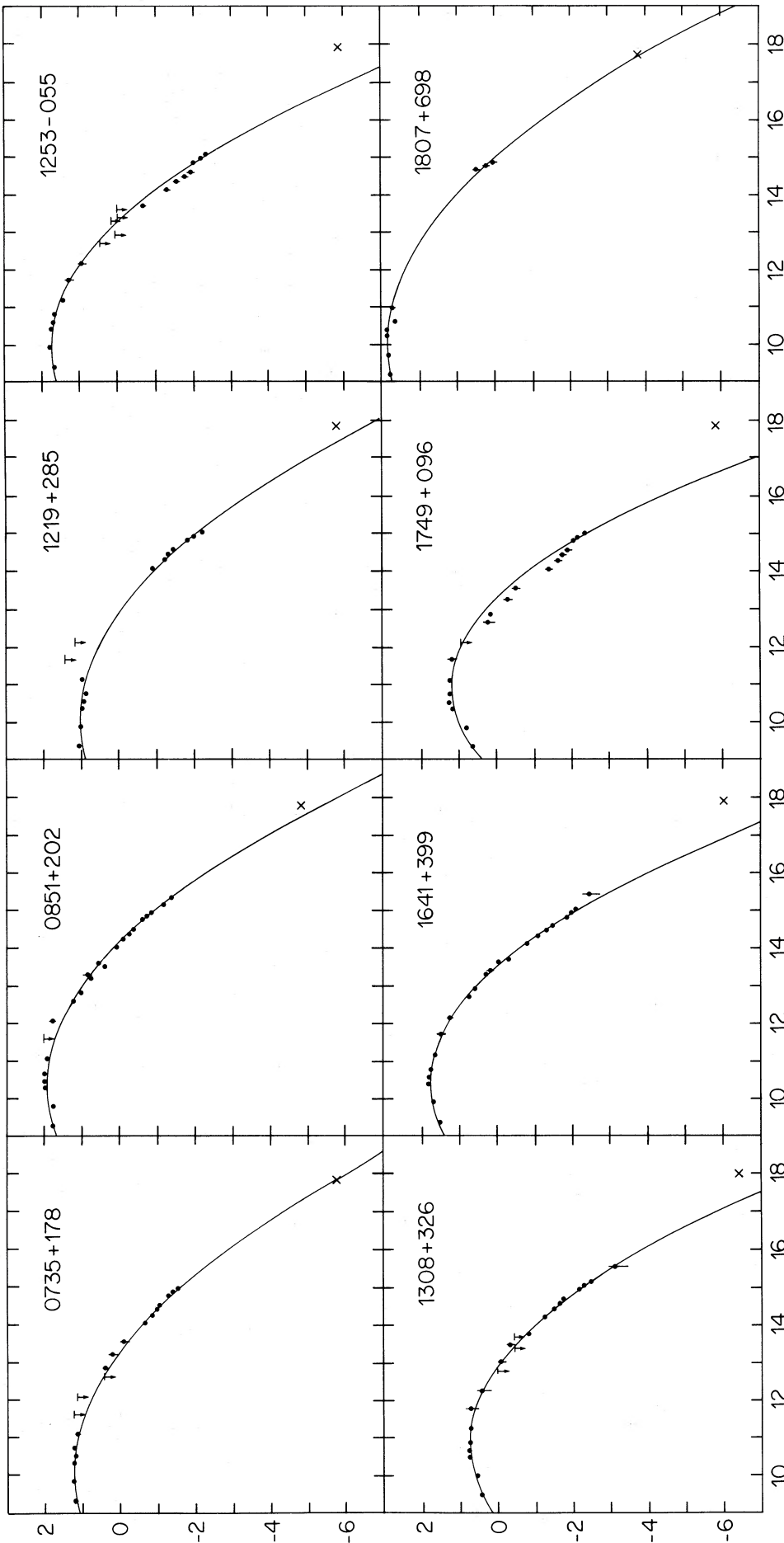


FIG. 4.—Broad-band spectra of the eight active sources for which X-ray data are available. The solid line is the best-fit parabola, extrapolated into the X-ray region. The X-ray point (shown as a cross) was *not* used to compute the fit. Our data are plotted as filled dots.

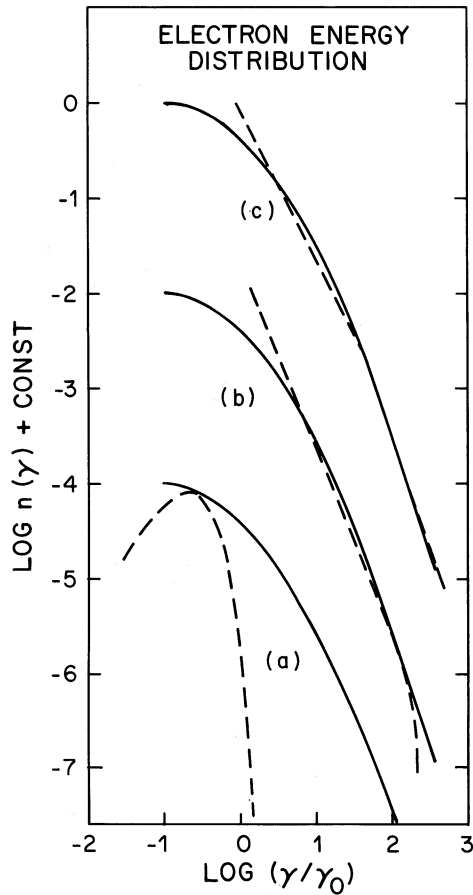


FIG. 5.—Selected electron energy distributions. Each of the solid curves is the same logarithmic parabola, which produces the average best-fit quadratic synchrotron emissivity (see eq. [1]). Also shown as dashed curves are (a) relativistic Maxwellian, (b) Fermi acceleration with energy loss (eq. [5]) truncated at low energies, and (c) broken power law truncated at low energies.

Maxwellian distribution is significantly too narrow to account for the broad-band spectra.

The spectral forms of sources, such as those observed here, are traditionally fitted by “broken” power laws. These data show clearly that such an interpretation is inadequate. However, true spectral breaks are unphysical because even the monoenergetic emissivity has a finite frequency spread. The emission spectrum from a distribution $n(\gamma)$ can be written in the form, $S(\nu) = \text{const} \int F(\nu, \gamma)n(\gamma)d\gamma$, which is recognized as a Fredholm equation of the first kind with a kernel function F . From the theory of such equations, the amount of structure or “information” contained in $n(\gamma)$ that can appear in $S(\nu)$ is determined by the smoothness of F and by the limits of integration. When the limits are wide and the kernel is smooth then structure in $n(\gamma)$, such as sharp breaks, is washed out by the integration, and one would not expect to see sharp breaks in $S(\nu)$. In fact, F has the form (Blumenthal and Gould 1970):

$$F(x) = x \int_x^\infty K_{5/3}(\gamma)d\gamma \cong 1.8x^{1/3}e^{-x}, \quad (4)$$

which has a half-power full width of 1.5 decades and a slowly falling exponential tail with substantial power at 3 decades. Calculations with this kernel demonstrates that a single-component energy distribution with a sharp break would

produce a spectrum with a smooth transition ~ 3 decades wide between the two straight lines of different slope which it approaches asymptotically.

It is therefore useful to compare the emissivity of a broken power-law energy distribution to the logarithmic parabola. Figure 5c shows a broken power-law with $s = 2.0$ at low energies and a break $\Delta s = 1.0$, at $\gamma/\gamma_0 = 30$, and a high-energy cutoff suggested in simple models for continuous power-law particle injection and synchrotron-Compton energy losses (Kardashev 1962). Figure 6 illustrates a “best fit” to the logarithmic parabola spectrum by the resulting synchrotron emissivity. A reasonable fit can be achieved except in the $\alpha = 0$ portion of the spectrum. However, in that region finite optical depths are likely, and VLBI observations tell us that the sources have complex structures. So it is reasonable to expect that a somewhat more sophisticated model which incorporates opacity effects will be needed to produce an adequate fit.

Finally, as an alternative to the broken power law we consider the particle distribution and associated synchrotron spectrum derived from first-order Fermi acceleration accompanied by escape and synchrotron losses. This resembles what one anticipates during acceleration by shocks (e.g., Bell 1978). The steady state particle distribution (assumed isotropic) can be

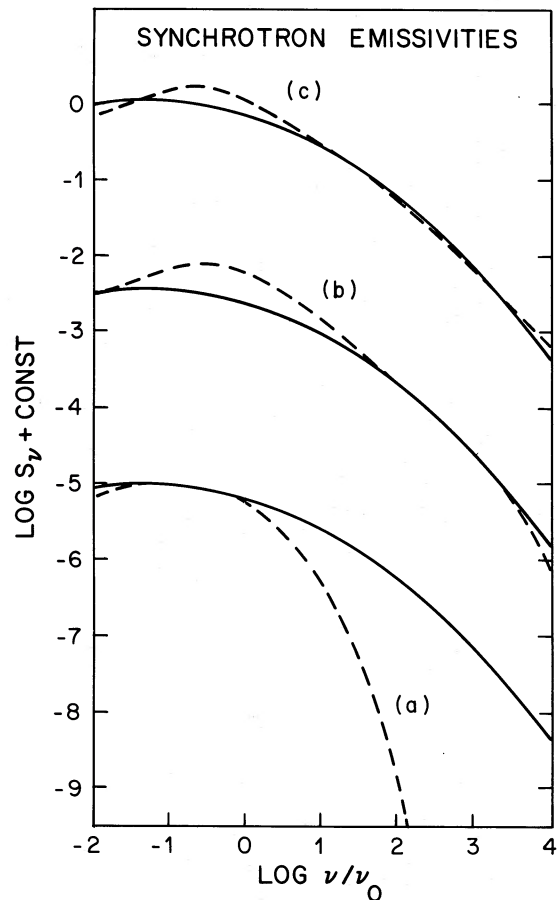


FIG. 6.—Synchrotron emissivities resulting from energy distributions in Fig. 5 (shown as dashed curves). Solid curves represent the average quadratic fits to the observed source spectra. The low frequency turnover in the other spectra depends upon the energy at which the energy spectra are truncated (or alternatively where the spectra become self-absorbed).

written

$$n(\gamma) \propto \gamma^{-(1+q)}(1 - \gamma/\gamma_1)^{(1-q)}, \quad (5)$$

where q is the ratio of escape to Fermi acceleration rates, while γ_1 is the energy at which Fermi energy gains are balanced by synchrotron losses. This distribution with $q = 2.5$ is shown in Figure 5 with the associated synchrotron spectrum in Figure 6. The comparison with a logarithmic parabola is similar to that for a broken power law. If opacity effects, which tend to reduce the emission at low frequencies, are combined with some kind of tapered source structure at centimeter wavelengths (see Jones *et al.* 1981), either model may provide an adequate fit to the data. This suggests that power-law energy distributions corrected for synchrotron losses may be a reasonable starting point in modeling these sources, provided that opacity can be expected to be significant in the submillimeter band. Other arguments derived from radio properties (e.g., Jones *et al.* 1983) and optical properties (e.g., Sitko *et al.* 1984) suggest this may be the case.

We now ask what physical conclusions can be drawn from the observed correlations between parameters of the parabolic fits for our active group, as discussed in § III(b) above. Detailed models of compact sources (e.g., Reynolds 1982) use a large number of parameters to describe their radiative and dynamical properties. The striking similarity among our observed spectra suggests that such parameters cannot be chosen freely from source to source. Either some of the parameters are universally fixed, or there are physical relationships between them which we have not yet isolated.

Even within any specific model (e.g., winds or jets), it appears that we should be able to pick at least four parameters independently, such as relativistic particle density (N), magnetic field strength (B), size (R), and shape [i.e., $N(r/R)$, $B(r/R)$]. Our data suggest that there are no more than two. On empirical and theoretical grounds, it has been often suggested that there is a limiting brightness temperature of order 10^{12} K. This is one example of a constraint which would force a reduction in the number of free parameters. Another possible constraint may be implied by the fact that the peak energy (νS_ν) occurs in a narrow range around 10^{14} Hz, as discussed above, even though the frequency of peak flux varies over a considerably broader range.

Given the small size of our source sample, we cannot yet separate the fundamental correlations from ones that arise indirectly. Our main point is that the observations show us that the relationships between active sources are simple ones. Therefore, theoretical models need to incorporate physically meaningful ways of reducing their number of independent parameters, either through feedback or regulation mechanisms or by severely restricting the range of allowable properties.

b) The "Control" Sample

The control sample, selected because of peaked radio spectra or low radio-to-optical flux ratios, are generally fitted very poorly by equation (1), as can be seen from Table 4. This is true despite the fact that all of them have large wavelength gaps in the data, which should allow more freedom to achieve a good fit. The classes of models which may describe the active sources therefore cannot apply to the control group, and we expect that these are physically distinct sets of sources, and not simply

extremes of a continuum. Although the data are spotty, the control sources are also distinguished by their low radio or optical polarizations (Rudnick and Jones 1982), or both. These characteristics also define our "anomalies" (admittedly after the fact), which are also poorly fitted by equation (1). In contrast to the active sources, there is thus no good evidence that the radio and optical emitting regions of the control sources are physically related.

Even within a more restricted wavelength range, samples of QSOs similar to our control sources show evidence for more than one component. Cutri *et al.* (1985) concluded, for a sample of "quiescent" QSOs, that even the infrared and variable optical continuum emissions arise from distinct sources. Such distinct components have also been identified from the shape of the continuum spectra, leading to models of UV thermal emission (e.g., Malkan and Sargent 1982), perhaps from a hot accretion disk (Shields 1978). The current work shows that distinct components will also be needed to explain the radio emission from these nonactive sources.

V. CONCLUSIONS

1. Active compact extragalactic sources, which have been selected on the basis of strong millimeter fluxes, have overall spectra which are well represented by functions with continuous curvature, such as parabolas. This suggests that emission from the radio to the ultraviolet is related in these sources.
2. Sharp spectral "breaks" are not observed, nor are they theoretically expected since any sharp break in energy space transforms to a more gradual curvature in frequency space.
3. In terms of simple physical models, adequate fits to the observed spectra can be obtained using either continuous particle injection and synchrotron losses, or first-order Fermi acceleration with escape and synchrotron losses. In each case, opacity starting at submillimeter wavelengths is necessary to reduce the long wavelength fluxes. Models using relativistic Maxwellian electron distributions do not fit the data well.
4. Observed correlations between the spectral fit parameters imply that active sources are related to one another in physically simple ways.
5. Fits to the spectra of "scrambled" pseudo-sources show that in the absence of good wavelength coverage, models of source spectra must be treated with caution, with derived parameters considered only as characteristic of the class.
6. Sources with peaked radio spectra or low radio-to-optical flux ratios do not appear to have continuously curving spectra and thus appear physically distinct from the active sample. They show low optical or radio polarizations, or both, and their radio and optical emissions may not be related.

For observing assistance and contributions of data we thank Richard Barvainis, Eric Becklin, Bill Cotton, B. Kevin Edgar, B. Ellis, Gary Grasdalen, Rick Howard, Wayne Kinzel, L. Lesyna, Tom Manley, Mike Werner, Paul Rhodes, M. Rowan-Robinson, and W. Z. Wisniewski. Bill Zumach gave programming support and Joel Baskin helped with the data reduction. M. Rowan-Robinson furnished useful comments on the text. This research was supported under grants AST 83-15949, AST 83-11973, AST 84-08740, and AST 81-14737 from the NSF, and NAG5-190 from NASA.

REFERENCES

- Angel, J. R. P., and Stockman, H. S. 1980, *Ann. Rev. Astr. Ap.*, **18**, 321.
 Baars, J. W. M., Genzel, R., Pauliny-Toth, I. I. K., and Witzel, A. 1977, *Astr. Ap.*, **61**, 99.
 Balonek, T. J. 1982, Ph.D. thesis, University of Massachusetts, Amherst.
 Balonek, T. J., and Dent, W. A. 1980, *Ap. J. (Letters)*, **240**, L3.
 Barvainis, R. 1984, Ph.D. thesis, University of Massachusetts, Amherst.
 Beichman, C. A., Neugebauer, G., Habing, H. J., Clegg, P. E., and Chester, T. J., eds. 1984, *Explanatory Supplement to the IRAS Catalogs and Atlases* (Pasadena: Jet Propulsion Laboratory).
 Bell, A. R. 1978, *M.N.R.A.S.*, **182**, 147.
 Blumenthal, G. R., and Gould, R. J. 1970, *Rev. Mod. Phys.*, **42**, 237.
 Bregman, J. N., et al. 1982, *Ap. J.*, **253**, 19.
 ———. 1984, *Ap. J.*, **276**, 454.
 ———. 1985, *Ap. J.*, **291**, 505.
 Burstein, D., and Heiles, C. 1982, *A.J.*, **81**, 1165.
 Cruz-Gonzalez, I., and Huchra, J. P. 1984, *A.J.*, **89**, 441.
 Cunningham, C. T., Ade, P. A. R., Robson, E. I., Nolt, I. G., and Radostitz, J. V. 1981, *Icarus*, **48**, 127.
 Cutri, R. M., Wisniewski, W. Z., Rieke, G. H., and Lebofsky, M. J. 1985, *Ap. J.*, **296**, 423.
 Elias, J. H., et al. 1978, *Ap. J.*, **220**, 25.
 Elias, J. H., Frogel, J. A., Matthews, K., and Neugebauer, G. 1982, *A.J.*, **87**, 1029.
 Ennis, D. J., Neugebauer, G., and Werner, M. 1982, *Ap. J.*, **262**, 460.
 Fogarty, W. G. 1975, *IEEE Trans.*, **AP-23**, 441.
 Glassgold, A. E., et al. 1983, *Ap. J.*, **274**, 101.
 Harvey, P. M., Wilking, B. A., and Joy, M. 1982, *Ap. J. (Letters)*, **254**, L29.
 Hayes, D. S. 1979, *Dudley Obs. Rept.*, No. 14, 297.
 Holm, A., and Rice, G. 1981, *NASA/IUE Newsletter*, No. 15, p. 74.
 Jones, T. W., and Hardee, P. E. 1978, *Ap. J.*, **228**, 268.
 Jones, T. W., Rudnick, L., Owen, F. N., Puschell, J. J., Ennis, D. J., and Werner, M. W. 1981, *Ap. J.*, **243**, 97.
 Kardashev, N. S. 1962, *Soviet Astr.—A.J.*, **6**, 317.
 Kondo, Y., et al. 1981, *Ap. J.*, **243**, 690.
 Kunkel, W. E., and Rydgren, A. E. 1979, *A.J.*, **84**, 633.
 Kurucz, R. L. 1979, *Ap. J. Suppl.*, **40**, 1.
 Landau, R., et al. 1983, *Ap. J.*, **268**, 68.
 Landau, R., Epstein, E. E., and Rather, J. D. G. 1980, *A.J.*, **85**, 363.
 Landolt, A. U. 1973, *A.J.*, **78**, 959.
 Ledden, J. E., and O'Dell, S. L. 1985, *Ap. J.*, **298**, 345.
 Madejski, G. M., and Schwartz, D. A. 1983, *Ap. J.*, **275**, 467.
 Malkan, M. A., and Sargent, W. L. W. 1982, *Ap. J.*, **254**, 22.
 Mufson, S. L., et al. 1984, *Ap. J.*, **285**, 571.
 Neugebauer, G., Oke, J. B., Becklin, E. E., and Matthews, K. 1979, *Ap. J.*, **230**, 79.
 Neugebauer, G., et al. 1984, *Ap. J. (Letters)*, **278**, L1.
 Phillips, R. B., and Mutel, R. L. 1980, *Ap. J.*, **236**, 89.
 Puschell, J. 1983, *Pub. A.S.P.*, **90**, 652.
 Reynolds, S. P. 1982, *Ap. J.*, **256**, 13.
 Robson, E. I., et al. 1983, *Nature*, **305**, 194.
 Roellig, T. P. L., and Houck, J. R. 1983, *Internat. J. Infrared and Millimeter Waves*, **4**, 299.
 Rudnick, L., and Jones, T. W. 1982, *Ap. J.*, **255**, 39.
 ———. 1983, *A.J.*, **88**, 518.
 Salonen, E., et al. 1983, *Astr. Ap. Suppl.*, **51**, 47.
 Sandage, A. 1973, *Ap. J.*, **180**, 687.
 Shields, G. A. 1978, *Nature*, **272**, 706.
 Sitko, M. L., Rudnick, L., Jones, T. W., and Schmidt, G. D. 1984, *Pub. A.S.P.*, **96**, 402.
 Sitko, M. L., Schmidt, G. D., and Stein, W. A. 1985, *Ap. J. Suppl.*, **59**, 323.
 Sitko, M. L., Stein, W. A., Zhang, Y.-X., and Wisniewski, W. Z. 1982, *Ap. J.*, **259**, 486.
 Spangler, S. R. 1980, *Ap. Letters*, **20**, 121.
 Tannanbaum, H., Wardle, J. F. C., Zamorani, G., and Avni, Y. 1983, *Ap. J.*, **268**, 60.
 Tokunaga, A. 1984, *A.J.*, **89**, 172.
 Tüg, H., White, N. M., and Lockwood, G. W. 1977, *Astr. Ap.*, **61**, 679.
 Ulich, B. L. 1981, *A.J.*, **86**, 1619.
 Werner, M. W., Neugebauer, G., Houck, J. R., and Hauser, M. G. 1978, *Icarus*, **35**, 289.
 Wills, B. J., et al. 1983, *Ap. J.*, **274**, 62.
 Worrall, P. M., et al. 1982, *Ap. J.*, **261**, 403.
 ———. 1984a, *Ap. J.*, **278**, 521.
 ———. 1984b, *Ap. J.*, **284**, 512.

P. CLEGG and S. HARRIS: Queen Mary College, Mile End Road, London E1 4NS, England, UK

B. GOLISCH: Mauna Kea Observatory, Institute for Astronomy, 177 Makaala Street, Hilo HI 96720

C. IMPEY: Division of Physics, Mathematics and Astronomy, Caltech, Pasadena, CA 91125

J. KENNY: University of Massachusetts, Department of Physics and Astronomy, Amherst, MA 01002

R. LANDAU, T. J. JONES, T. W. JONES, J. PEDELTY, and L. RUDNICK: University of Minnesota, Department of Astronomy, 116 Church Street SE, Minneapolis, MN 55455

G. NEUGEBAUER, K. MATTHEWS, and J. H. ELIAS: Palomar Observatory, California Institute of Technology, Pasadena, CA 91125

T. ROELLIG: MS 245-6, NASA-Ames Research Center, Moffett Field, CA 94035

E. SALONEN and S. URPO: Helsinki University of Technology, Radio Laboratory, Otakaari 5A, 02150 Espoo, Finland

G. SCHMIDT: Steward Observatory, University of Arizona, Tucson, AZ 85721

M. L. SITKO: Kitt Peak National Observatory, P.O. Box 26732, Tucson, AZ 85726